Supplementary information

Functional differences between neurotransmitter binding sites of muscle acetylcholine receptors

Short Title:

Agonist binding sites of muscle AChR

Authors:

Tapan K Nayak[a], *Iva Bruhova[a], *Srirupa Chakraborty[a,b], Shaweta Gupta[a], Wenjun Zheng[b], Anthony Auerbach[a†]

[a]Department of Physiology and Biophysics, State University of New York at Buffalo, Buffalo, NY, 14214

[b]Department of Physics, State University of New York at Buffalo, Buffalo, NY, 14260

Corresponding author:

Anthony Auerbach, Department of Physiology and Biophysics,

SUNY at Buffalo, Buffalo, NY 14214

Phone: 716-829-2435;

Fax: 716-829-2569

Email: auerbach@buffalo.edu

Methods

Cycle

The free energy of the agonist affinity change was estimated by using a thermodynamic cycle (Fig. S1). The resting↔active conformational change occurs both in the absence of agonists (equilibrium constant E_0) and when one or two agonists are bound (E_1 or E_2). The total free energy change of the gating isomerization (product minus reactant; kcal/mol, 23 °C) is $G_n = -0.59 \times \ln(E_n)$, where n is the number of bound agonists. The free energy of the agonist affinity change at one binding site (ΔG_{B1}) is the difference between the high-affinity (HA) and low-affinity (LA) binding energy, $\Delta G_{B1} = G_{HA} - G_{LA}$. From microscopic reversibility, $\Delta G_{B1} = G_1 - G_0$ for a 1-site receptor and $(\Delta G_{B1} + \Delta G_{B2}) = G_2 - G_0$ for a 2-site receptor. We measured the gating rate constants E_0, E_1 and E_2 (G_0, G_1 and G_2) and calculated ΔG_{B1} and $(\Delta G_{B1} + \Delta G_{B2})$ using the above relationships.

For different agonists and mutations of the aromatics at the binding sites, the changes in HA and LA binding energies are correlated (1, 2). For these perturbations, the HA energy change was in all cases about twice that of LA energy change ($\Delta G_{HA} \approx 2\Delta G_{LA}$). Hence, in muscle AChRs $\Delta G_{B1} \approx G_{LA}$. The LA equilibrium dissociation constant of a resting AChR (K_d) can be derived from the relationship $\Delta G_{B1} = +0.59 \times \ln(K_d)$. ΔG_{B1} is a quantitative index of both the liganded gating equilibrium constant ('efficacy') and the resting equilibrium dissociation constant ('affinity').

Electrophysiology

The gating equilibrium constants (E_n) and corresponding free energies (G_n) were estimated by using single-channel patch-clamp electrophysiology. Mutations were incorporated into AChR subunits by using the *QuickChange* site-directed mutagenesis kit (Agilent Technologies, CA), were verified by nucleotide sequencing and expressed in HEK cells by transient transfection.

Single-channel currents were recorded in the cell-attached configuration (23 °C). The bath solution was (mM): 142 KCl, 5.4 NaCl, 1.8 $CaCl_2$, 1.7 $MgCl_2$, 10 HEPES/KOH, pH 7.4 and the pipette solution was: 137 NaCl, 0.9 $CaCl_2$, 2.7 KCl, 1.5 KH_2PO_4, 0.5 $MgCl_2$, and 8.1 Na_2HPO_4, pH 7.3. To estimate E_2, agonists at saturating concentration (100 mM, which is $>10\times K_d$) were added to the pipette solution. The agonists were acetylcholine (ACh), carbamylcholine (CCh), tetramethylammonium (TMA) or choline (Cho). At high concentrations, agonists resulted in significant channel-block at -100 mV, which was eliminated by depolarization to +70 mV. In order to engineer the gating rate constants to be in a range suitable for kinetic analysis we sometimes added background mutations that only changed E_0 (G_0) but had no effect on ΔG_{B1} (see below).

Currents from individual AChRs associated with the resting↔active 'gating' isomerization occurred in clusters separated by silent periods associated with sojourns to longer-lived desensitized states (3) (Fig. 2a). Kinetic analyses of intervals within clusters were performed by using QUB (4). To estimate the rate constants, clusters of shut↔open activity were selected and idealized into noise-free intervals by using the segmental k-means algorithm after digitally low-pass filtering at 12 kHz. The forward (f_n) and backward (b_n) gating rate constants were estimated from the idealized intra-cluster interval durations by fitting the data to a simple kinetic shut↔open model using a maximum-interval likelihood algorithm after imposing a dead time of 20-50 μs. Occasionally, an additional shut state, presumably representing a short-lived desensitized state, was added to the kinetic scheme. The gating equilibrium constant was calculated from the ratio of the rate constants. $E_n=f_n/b_n$.

Protein engineering

Many AChR mutations away from the agonist sites only influence the unliganded gating energy, G_0 (5). Because G_0 is part of the ΔG_{B1} calculation, it was essential to measure G_0 experimentally for *every* construct. G_0 in WT AChRs at -100 mV is +8.3 or +9.9 kcal/mol (E_0=7.4 or 0.52 x10^{-7}) (6), adult or fetal, which in both cases is too unfavorable to allow cluster formation. In order to estimate ΔG_0 for each binding site mutation, we added background mutations that made G_0 more favorable for opening, to known extents, but had no effect on binding (Table S9). In selecting the backgrounds we chose those that were energetically independent, so that the aggregate ΔG_0 was the sum of the ΔG_0 values for each perturbation. The observed G_0^{mut} was corrected for the background to estimate its value at a reference condition (-100 mV, 23 ºC, WT) (7).

For example, the observed gating rate constants for the background construct fetal+βT456I+δI43H (V_m=+70 mV), obtained by fitting interval durations at saturating CCh, were $f_2^{CCh,bkg}$=1316±58 s^{-1} and $b_2^{CCh,bkg}$=811±27 s^{-1} (Fig. 2a). Each background mutation decreases f_0 by 1.3 or 0.9-fold, and increases b_0 by 0.3 or 3.2-fold, respectively. Depolarization by +170 mV decreases f_0 by 5-fold and increases b_0 by 0.6-fold. Hence, the net effect of all perturbations combined (relative to WT at -100 mV) is to decrease f_0 by 5.8-fold and to increase b_0 by 0.57-fold. Multiplying the observed rate constants by these factors yields (for WT, fetal AChRs at -100 mV) f_2^{CCh}=7697 s^{-1} and b_2^{CCh}=467 s^{-1}, or E_2^{CCh}=16.5. From the relationship G_2=-0.59lnE_2 we estimate that under these conditions G_2^{CCh}=-1.65 kcal/mol. $G_0^{WT,fetal}$=+9.9 kcal/mol, so we use $(\Delta G_{B1}+\Delta G_{B2})^{CCh}=G_2^{CCh}-G_0^{WT}$ to calculate $(\Delta G_{B1}+\Delta G_{B2})^{CCh}$=-11.6 kcal/mol (Table S1). The

approximate error limit on the energy estimates is ±0.4 kcal/mol (a ~2-fold change in equilibrium constant) (8).

Single site knockouts

In order to study AChRs having just one functional binding site we added mutations to the ε, γ, δ subunits that eliminate agonist activation at the mutated site (9). To make an αγ- or αε-only AChR we added δP123R, and to make an αδ-only AChR we added ε/γP121R, sometimes in combination with γW55R. In addition to reduce agonist activation, these background mutations also alter G_0. Therefore, E_1 *and* E_0 were determined for each knock-out construct, as described above.

Molecular dynamic simulations

a. Model preparation and ligand docking. The starting models of the muscle AChR for our simulations were built in two ways. First, we modeled dimers of the extracellular domains (ECD) (residues 17-209) of an α and a non-α subunit (δ, ε or γ) using the structure of *Aplysia californica* ACh binding protein (AChBP) bound to epibatidine (PDB ID: 2BYQ; (10)). The ECD of α, δ, ε and γ subunits of muscle AChRs share ~45-52% homology and ~23% sequence identity, with *A. californica* AChBP. The sequence alignment was based on the multiple-sequence alignment from ClustalX as shown in Hansen et al, 2005 (10) that ensures the correct alignment of sequentially conserved residues (Table S10). Second, we built a hetero-pentameric AChR by structurally aligning the dimers to the *Aplysia* AChBP (2BYQ). αδ and αγ dimers were aligned to chains A-E and C-B. Chain D was left unchanged.

Homology models were constructed by using the ZMM program (http://www.zmmsoft.com), which employs the Monte Carlo minimization algorithm (MCM) to search for energetically favorable conformations (11). The dimer models were MC-minimized until 2000 consecutive energy minimizations did not decrease the apparent global minimum. During energy minimization of the dimer models, the α carbons of the protein were constrained to the template structure by pins, which are flat-bottom energy constraints that allow atoms to deviate penalty-free up to 1 Å from the template but impose a penalty of 10 kcal/mol/Å for larger deviations. For docking, we searched for the optimal positions and orientations of ACh using a multi-MCM protocol (12, 13). For further details regarding the modeling methods, see Bruhova *et al* (14).

b. MD simulations. The three ACh-dimer complexes (αδ, αε and αγ) with 1 ACh molecule, and the hetero-pentamer model with 2 ACh molecules were further optimized and equilibrated by using energy minimization and MD simulation. Each of the systems was solvated in a water box using the TIP3P water model (15) and the box was extended at least 10 Å from the periphery of the protein in each dimension. Na^+ and Cl^- ions were added to neutralize the system and bring it to an ionic concentration of 150 mM each.

The simulations were conducted using NAMD version 2.8 (16), with CHARMM27 force field (17). First, a 20,000-step minimization was done using the steepest descent method, and with gradual release of restraints on the protein backbone. Then the systems were subjected to 20 ns MD simulation (50 ns for the heteropentamer) performed in the NPT ensemble. The Nosé-Hoover method (18) was used with a temperature of 300 K and a pressure of 1 atm. In the dimer simulations, harmonic restraints (force constant=1 kcal/mol/$Å^2$) were applied on the backbone atoms of residues which were >20 Å away from the ACh molecule at the binding site. These

restraints maintain the global backbone conformation of the model while allowing relaxation of all side chains and the residues in the key loops of the agonist site. In the pentamer simulations, there were no restraints imposed on the backbone atoms.

Periodic boundary conditions were applied. A 10 Å switching distance and a 12 Å cutoff distance were used for non-bonded interactions. The particle mesh Ewald (PME) method (19) was used to calculate long-range electrostatic interactions. The SHAKE algorithm (20) was used to constrain bond lengths of hydrogen-containing bonds, which allows a time step of 2 fs for MD simulations. Four MD simulation trajectories were obtained for each of the models. The coordinates of the systems were saved every 1 ps during MD simulations.

c. Calculation of ACh-protein binding free energy. The ACh-protein binding free energy was calculated using a continuum solvent model (21). The simulated binding free energy, ΔG_{B1}, is expressed as $\Delta G_{np}+\Delta G_{elec}$. Here, the nonpolar contribution ΔG_{np} ($=\lambda E_{vdW}$) is empirically written as a fraction ($\lambda<1$) of the van der Waals (vdW) interaction energy. λ is small because the gain in favorable vdW interaction energy between ACh and protein is largely compensated by a loss of vdW interaction energy between the free protein/ACh with water. We used the empirically-estimated value of $\lambda = 0.17$ in (21). The ACh molecule remained close to its equilibrium position at all binding sites, with the nitrogen deviating by an average of 1.0±0.4 Å.

ΔG_{elec} was calculated using the Poisson−Boltzmann (PB) method (22, 23) where a probe radius of 1.4 Å was used to define the molecular surface corresponding to the dielectric boundary. The salt concentration was set to 140 mM, corresponding to the buffer condition for experimental measurements. All the PB calculations were performed using the PBEQ module (24) of the CHARMM program (25). Each PB calculation was conducted by using bilinear interpolation to

construct the boundary potential. The atomic Born radii used were previously calibrated and optimized to reproduce the electrostatic free energy of the 20 amino acids in MD simulations with explicit water molecules (26). The binding energy calculations were done on snapshots extracted every 20 ps over the last 10 ns of each trajectory for the dimer-ACh model and the last 40 ns for the pentamer-ACh model. The ensemble for each state, therefore, contained 2,000 and 8,000 snapshots for the dimer and pentamer, respectively, which were used to perform all quantitative analyses.

We also calculated the binding energy using AUTODOCK-4 (epdb module; (27)) and the MMPBSA method (28) for comparison. In MMPBSA, a non-polar surface area term is added and the vdW term is unscaled resulting in over-estimation of the energy (29). The binding energy estimates by all methods are summarized in Table S6.

d. Structural parameters and dynamics. For structural analyses, the geometric centers of the aromatic rings of interest and the ACh quaternary amine (QA) nitrogen were used as reference points. The structural analyses were done using the last 10 and 40 ns of each trajectories for the dimer and hetropentamer simulations, respectively.

Angle between Tryptophans: The angle between the αW149 and W55 indole rings was defined as the angle between the perpendiculars to the planes of the rings for each residue.

*Volume***:** The pocket surrounding the quaternary ammonium (QA) group of CCh in AChBP is outlined by αW149, αY93, αY190, αY198 and W55 in the non-α subunit (Fig. 1b). The volume of this pocket was estimated by joining the centroids of the aromatic rings to form two adjoining tetrahedrons (Fig. S7b). The volume of each of the tetrahedrons was estimated using the 3-simplex determinant method from the coordinates of the vertices.

Hydrogen bonds, electrostatic and cation-π interactions: We used the following geometric criteria: H-bond, a donor−acceptor distance of <3.5 Å and a donor-hydrogen-acceptor angle of ≥60°; electrostatic interaction, a maximal distance of 6 Å between two charged atoms; cation-π interaction, a distance cutoff of less than 6 Å between the ACh QA nitrogen and the geometric center of the aromatic ring, and an angle cutoff of less than 45° between the normal to the ring plane and the vector joining the ring center and the ACh nitrogen (30). We used VMD program (31) to identify and calculate the above parameters in the last 10 ns ensemble for the dimer models**.**

RMSF: To compare the flexibility of the ligand-binding interface between the three sites, we performed root-mean-square fluctuation (RMSF) analysis based on the last 10 ns of the MD simulations of the dimer models. RMSF of Cα atoms of each residue was calculated with respect to the mean of the ensemble using VMD version-1.9.

Table S1. Rate/equilibrium constants and free energies for AChRs with 2 active agonist binding sites

agonist	WT	f_2	b_2	E_2	G_2^{obs}	G_0^{WT}	$\Delta G_{B1}+\Delta G_{B2}$	citation
ACh	fetal	24020	410	58.7	-2.4	9.9	-12.3	(6)
	adult	65850	2595	25.4	-1.9	8.3	-10.2	(7)
CCh	fetal	7697 (335)	467 (14)	16.5 (0.9)	-1.7[a] (0.03)	9.9	-11.6 (0.3)	
	adult	8603	1612	5.33	-1.0	8.3	-9.3	(7)
TMA	fetal	1687 (248)	403 (37)	4.2 (0.7)	-0.8[a] (0.09)	9.9	-10.7 (0.3)	
	adult	5233	2057	2.54	-0.5	8.3	-8.8	(7)
Cho	fetal	50 (2.6)	821 (25)	0.06 (0.01)	1.7[c] (0.09)	9.9	-8.2 (0.3)	
	adult	101	2181	0.046	1.8	8.3	-6.5	(7)

f_2 (s^{-1}) and b_2 (s^{-1}) are the diliganded forward and backward gating rate constants (±S.E.M.; $n \geq 3$ patches); $E_2=f_2/b_2$; ΔG_2 (kcal/mol)=-0.59*ln(E_2). G_0 is the unliganded (intrinsic) gating energy at -100 mV. The net agonist energy from two sites combined is $\Delta G_{B1}+\Delta G_{B2}=G_2-G_0$. Superscript letters indicate background mutations (see Table S9).

Table S2. Agonist free energies for AChRs having only 1 functional WT binding site

agonist	site	G_1^{obs}	G_0^{bkg}	ΔG_{B1}
ACh	αγ (6)	2.8	9.9	-7.1
	αδ (9)	4.6	9.9	-5.3
	αε (9)	3.2	8.3	5.1
CCh	αγ	-0.4	7.1[l]	-7.5
	αδ	1.7	6.7[f]	-5.0
	αε	1.2	6.2[f]	-5.0
TMA	αγ	1.0	7.1[l]	-6.1
	αδ	-0.6	3.6[q]	-4.2
	αε	-0.7	3.1[q]	-3.8
Cho	αγ	2.6	7.1[l]	-4.5
	αδ	1.4	4.9[j]	-3.5
	αε	2.3	5.0[j]	-2.7

All energies are kcal/mol. To facilitate 1-site binding energy measurements, mutations that only changed G_0 without affecting binding were used as backgrounds. $G_0^{bkg} = G_0^{WT} + \Delta G_0^{\Delta Vm} + \Delta G_0^{muts}$, where $\Delta G_0^{\Delta Vm}$ and ΔG_0^{muts} are the effects of voltage and background mutation(s) on G_0, respectively. A list of the backgrounds is given in Table S9. For different agonists, the net 1-site agonist energy $\Delta G_{B1} = G_1 - G_0^{bkg}$. Superscript letters, backgrounds (Table S9).

Table S3. Effects of mutations of Trp residues on the agonist free energy

position	mutated site	Mut	agonist	G_2^{obs}	G_0^{bkg}	$\Delta G_{B1}+\Delta G_{B2}$	other site	ΔG_{B1}^{mut}	$\Delta\Delta G_{B1}^{mut}$
W55	αγ	A	ACh	-0.11	2.7[u]	-2.8	KO	-2.8	4.4
				0.3	7.4[e]	-7.1	WT	-2.1	5.1
			Cho	-1.5	0.6[v]	-2.1	KO	-2.1	2.4
				1.9	7.4[e]	-5.5	WT	-1.9	2.6
	αε		ACh	1.9	6.0[i]	-4.1	KO	-4.1	1.0
				-0.8	8.2	-9.0	WT	-3.8	1.3
	αδ			1.6	7.2[g]	-5.6	KO	-5.6	-0.3
				-1.7	8.8	-10.5	WT	-5.4	-0.1
	αγ+αδ			0.4	8.0[d]	-7.6	-	-2.4	4.8
	αγ	F		0.5	7.3[e]	-6.8	KO	-6.8	0.4
	αε			0.2	5.5[k]	-5.3	KO	-5.3	-0.2
	αδ			1.3	6.4[g]	-5.1	KO	-5.1	0.1
	αγ	Y		-1.9	6.7[g]	-8.6	WT	-3.5	3.6
	αε								1.5[(32)]
	αδ								0.6[(32)]
αW149	αγ	A	ACh	-0.5	3.7[u]	-4.2	KO	-4.2	3.0
	αε			1.6	4.3[p]	-2.7	KO	-2.7	2.4
	αδ			0.8	3.7[s]	-2.9	KO	-2.9	2.4
	αγ+αδ			0.08	7.9[k]	-7.8	-	-2.5	-4.7

Agonist energies (kcal/mol) for Ala (A), Phe (F) and Try (Y) mutations at W55 and αW149 positions were estimated in AChRs with only 1-functional binding site (other site knocked out; KO) or with the companion site as the WT. The energy from the mutated site (kcal/mol) is ΔG_{B1}^{mut} and the change in agonist energy due to the mutation is $\Delta\Delta G_{B1}^{mut}=\Delta G_{B1}^{mut}-\Delta G_{B1}^{WT}$. Superscript letters, backgrounds (Table S9).

Table S4. Effect of mutations of α subunit Tyr residues on the agonist free energy

position	mutated site	mut	G_2^{obs}	G_0^{bkg}	$\Delta G_{B1}+\Delta G_{B2}$	other site	ΔG_{B1}^{mut}	$\Delta\Delta G_{B1}^{mut}$
αY93	αγ	A	-0.5	3.9[t]	-4.4	KO	-4.4	2.8
	αε+αδ (33)	A	0.3	8.4	-8.1	-	-4.05*	1.05
	αγ	F	1.7	8.1[h]	-6.4	KO	-6.4	0.8
	αε+αδ (33)	F	0.2	9.6	-9.4	KO	-4.7*	0.4
αY190	αγ	A	0.1	3.9[u]	-3.8	KO	-3.8	3.4
	αε+αδ (33)	A	5.8	8.4	-2.6	-	--1.3*	3.8
	αγ	F	2.2	7.8[h]	-5.6	KO	-5.6	1.6
	αε+αδ (33)	F	2.3	8.7	-6.4	-	-3.2*	1.9
αY198	αγ	A	1.0	6.2[u]	-5.2	KO	-5.2	2.0
	αε+αδ (33)	A	2.1	8.3	-6.2	-	-3.1*	2.0
	αγ	F	-0.8	6.8[l]	-7.6	KO	-7.6	-0.4
	αε+αδ (33)	F	-1.6	8.4	-10.0	-	-5.0*	0.1

ACh binding energies (kcal/mol) for A and F mutants of Tyr residues in the α-subunit. For the adult receptor, the agonist energies were previously estimated in AChRs with 2-WT binding sites (33). We assumed the αδ and αε sites to be independent and equivalent, so for these cases $\Delta G_{B1}^{mut} = \Delta G_{B2}/2$ (indicated by *). Superscript letters, backgrounds (Table S9).

Table S5. Free energy coupling between γW55 and aromatic residues in the α subunit

Side chain pair		mut	G_2^{obs}	G_0^{bkg}	$\Delta G_{B1}+\Delta G_{B2}$		$\Delta\Delta G_{B1}^{mut}$	coupling energy
γW55	αY93	A	0.7	2.8[t]	-2.1	KO	5.1	-2.1
	αW149		2.2	2.9[u]	-0.7		6.5	-1.0
	αY190		2.2	3.6[u]	-1.4		5.8	-2.0
	αY198		1.9	2.8[u]	-0.9		6.3	-0.1
	αY93	F	2.1	7.7[h]	-5.6		1.6	+0.4
γW55A	αY190	F	2.0	3.9[u]	-1.9		5.3	-0.7

Coupling free energies are for A-A, A-F and F-F mutation pairs (the agonist was ACh). The coupling energy (kcal/mol) is: (change in ΔG_{B1} for the mutation pair)-(sum of the changes in ΔG_{B1} for individual mutations). Superscript letters, backgrounds (Table S9).

Table S6. Ligand binding energy calculated from MD simulations

site	unscaled E^{vdW}	ΔG^{Elec}	ΔG_{B1}(continuum -solvent)	ΔG_{B1} (MMPBSA)	ΔG_{B1} (Autodock)	ΔG_{B1} (experiment)
dimer-ACh complex						
αδ	-15.7 (2.8)	-1.3 (0.3)	-4.0 (0.5)	-18.8 (2.8)	-3.4 (0.6)	-5.3
αε	-16.1 (2.9)	-1.1 (0.4)	-3.8 (0.6)	-19.0 (2.9)	-3.3 (0.7)	-5.0
αγ	-22.2 (2.8)	-1.4 (0.3)	-5.2 (0.5)	-35.4 (2.7)	-4.8 (0.7)	-7.1
heteropentamer-ACh complex						
αδ	-15.5 (2.6)	-0.9 (0.35)	-3.5 (0.5)			-5.3
αγ	-21.9 (2.4)	-1.5 (0.3)	-5.2 (0.4)			-7.1

Simulated ACh binding energy, $\Delta G_{B1}{}^{ACh}$ (kcal/mol) (±S.D.), was calculated by the continuum solvent model, MMPBSA method or by using the epdb module of Autodock (see Methods). Simulated $\Delta G_{B1}{}^{ACh}$ is the sum of the electrostatic (ΔG^{Elec}) and the scaled van der Waal energy (E^{vdW}) components. $\Delta G(\text{continuum solvent})=\Delta G^{Elec}+\lambda E^{vdW}$, where λ is an empirically determined scaling factor (=0.17). Notice that the difference in ΔG_{B1} between αγ vs. αε or αδ is similar irrespective of the method. Also note the consistency in ΔG_{B1} between dimer and pentamer simulations. The experimentally-measured ΔG_{B1} values are from single-channel electrophysiology.

Table S7. Structural parameters from MD simulations

Parameter	αδ	αε	αγ
dimer-ACh complex			
Trp angle (degree)	68.7 ± 23.7	40.04 ± 17.1	89.11 ± 16.6
Ligand pocket volume (Å^3)	115.3 ± 18.7	131.9 ± 30.9	92.80 ± 16.1
heteropentamer-ACh complex			
Trp angle (degree)	65.7±18.6		82.6 ± 7.2
Ligand pocket volume (Å^3)	101±17		77 ± 6

Trp angles: the angle between the normals to the aromatic rings of W55 and W149. The αγ site is the most-orthogonal. The volume of the binding pocket is the smallest in αγ, indicating compactness. Values are ±S.D.

Table S8. ACh distances from aromatic residues in the binding pocket

a.

position	αδ	αε	αγ
dimer-ACh complex			
γW55	9.7 (1.4)	8.8 (2.8)	7.5 (1.5)
αY93	9.2 (2.8)	8.7 (3.7)	6.5 (1.5)
αW149	7.3 (1.7)	7.5 (3.2)	5.0 (0.6)
αY190	6.0 (2.5)	8.8 (2.5)	5.2 (0.8)
αY198	6.3 (1.5)	6.6 (2.7)	5.1 (0.6)
heteropentamer-ACh complex			
γW55	9.2 (1.2)		7.2(1)
αY93	10.3 (3.2)		6.3 (0.7)
αW149	7.9 (1.5)		4.7 (0.3)
αY190	6.7 (1.4)		5.6 (0.3)
αY198	6.0 (1.3)		4.6 (0.3)

b.

position	αδ	αε	αγ
dimer-ACh complex			
αY93	8.0 (2.8)	7.4 (3.8)	5.6 (1.3)
αY190	6.0 (2.2)	8.3 (2.4)	4.8 (0.8)
αY198	6.2 (1.5)	6.6 (2.4)	5.3 (1)
heteropentamer-ACh complex			
αY93	9.3 (3.3)		4.7 (0.9)
αY190	6.4 (1.7)		5.9 (0.6)
αY198	5.5 (0.8)		4.8 (0.4)

a. Average (S.D.) distances (Å) are between the geometric center of aromatic residues and the QA of ACh. b. Average (S.D.) distances are between the –OH of the tyrosines and the QA of ACh. In general, the average distances are smaller at αγ vs αε/αδ.

Table S9. Unliganded gating free energies: backgrounds and mutants

constructs	ΔG_0^{bkg} (kcal/mol)	Citation		Mutants	ΔG_0^{mut} (kcal/mol)	Citation
βT456I δI43H[a]	0.6	(6)		δP123R	0.31	(6)
βT456I[b]	-0.6	(34)		εP121R	0.9	(9)
βT456I δI43Q[c]	-1.2			γW55A	-0.42	
αS269I[d]	-2.8	(35)		εW55A	-0.16	(32)
αA96V[e]	-3.0	(36)		δW57A	0.4	(32)
αD97A εS450W[f]	-3.0			γW55F	-0.6	
αA96V βT456I[g]	-3.6			εW55F	-0.38	(32)
βV266A[h]	-3.7	(8)		δW57F	-0.3	(32)
αS269I δI43Q[i]	-3.7			αY93A[γ]	-0.65	
αP272A βT456I[j]	-3.7			αY93F[γ]	0.67	
αA96V δI43Q[k]	-3.9			αW149A[γ]	0.5	
βL262S[l]	-4.0	(8)		αW149A[ε/δ]	-0.82	
αP272A δI43Q[m]	-4.0			αY190A[γ]	0.78	
βL262S δI43Q[n]	-4.4			αY190F[γ]	0.39	
αA96V εE181T εL269F[p]	-6.1	(37)		αY198A[γ]	-0.46	
αD97A εL269F[q]	-6.1			αY198F[γ]	-0.37	
βL262Q δL265Q[r]	-6.7					
αA96V δV269A[s]	-6.8					
αA96V βV266A[t]	-7.2	(6)				
βL262S δL265S[u]	-7.6	(8)				
αA96V βL262S δL265S[v]	-10.2					

Table S10. Multiple sequence alignment of subunits of muscle AChR and *A. californica* AChBP

```
AChR mouse alpha        17 SVVRPVEDHREIVQVTVGLQLIQLINVDEVNQIVTTNVRLKQQWVDYNLKWNPDDYGGVK 76
AChR mouse delta        19 KDLRPVARKEDKVDVALSLTLSNLISLKEVEETLTTNVWIDHAWVDSRLQWDANDFGNIT 78
AChR mouse epsilon      17 PECRPVRRPEDTVTITLKVTLTNLISLNEKEETLTTSVWIGIDWHDYRLNYSKDDFAGVG 76
AChR mouse gamma        17 PHLRPAERDSDVVNVSLKLTLTNLISLNEREEALTTNVWIEMQWCDYRLRWDPKDYEGLW 76
AChBP Aplysia           17 SPMYPGPTKDDPLTVTLGFTLQDIVKADSSTNEVDLVYYEQQRWKLNSLMWDPNEYGNIT 76
                                *     : : ::: . * :::. ..  : :         *    * :. .:: .:

AChR mouse alpha        77 KIHIPSEKIWRPDVVLYNNADGDFAIVKFTKVLLDYTGHITWTPPAIFKSYCEIIVTHFP 136
AChR mouse delta        79 VLRLPPDMVWLPEIVLENNNDSSFQISYACNVLVYDSGYVTWLPPAIFRSSCPISVTYFP 138
AChR mouse epsilon      77 ILRVPSEHVWLPEIVLENNIDSQFGVAYDSNVLVYEGGYVSWLPPAIYRSTCAVEVTYFP 136
AChR mouse gamma        77 ILRVPSTMVWRPDIVLENNVDSVFEVALYCNVLVSPDGCIYWLPPAIFRSSCSISVTYFP 136
AChBP Aplysia           77 DFRTSAADIWTPDITAYSSTRP-VQVLSPQIAVVTHDGSVMFIPAQRLSFMCDPTGVDS- 134
                            :: ..  :* *::.  ..    . :     .::   * : : *.      *    .

AChR mouse alpha       137 FDEQNCSMKLGTWTYDGSVVAINPESDQP-----------DLSNFMESGEWVIKEARGW 184
AChR mouse delta       139 FDWQNCSLKFSSLKYTAKEITLSLKQEEENNRSYPIEWIIIDPEGFTENGEWEIVHRAAK 198
AChR mouse epsilon     137 FDWQNCSLIFRSQTYNAEEVEFIFAVDDD---GNTINKIDIDTAAFTENGEWAIDYCPGM 193
AChR mouse gamma       137 FDWQNCSLIFQSQTYSTSEINLQLSQED----GQAIEWIFIDPEAFTENGEWAIRHRPAK 192
AChBP Aplysia          135 EEGATCAVKFGSWVYSGFEIDLKTDTDQV-----------DLSSYYASSKYEILSATQT 182
                            :  .*:: : :  *    : :    ::            *   :  ..:: *

AChR mouse alpha       185 KHWVFYSCCPTTPYLDITYHFVMQRL 210
AChR mouse delta       199 LNVDPSVPMDSTNHQDVTFYLIIRRK 224
AChR mouse epsilon     194 IRRYEGGSTEGPGETDVIYTLIIRRK 219
AChR mouse gamma       193 MLLDSVAPAEEAGHQKVVFYLLIQRK 218
AChBP Aplysia          183 RQVQHYSCCPEP-YIDVNLVVKFRER 207
                                .   .:   . ::.
```

Aromatic residues of the ACh-binding pocket that contribute significantly to ΔG_{B1}^{ACh} are highlighted (Fig. 1b). Comparable alignment results were obtained by using ClustalX, Modeller, and ZMM sequence alignment tools.

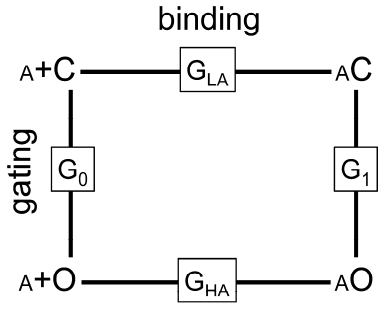

Fig. S1. Thermodynamic cycle. Thermodynamic cycle for AChRs having only one functional agonist binding site. C and O represent the global, 'resting' and 'active' state structure and A is the agonist (a small structural perturbation). The free energy difference in the vertical axes (O minus C) is G_n, where n is the number of bound agonists. Agonists bind with a low affinity (LA) to C and a high affinity (HA) to O, with corresponding free energy differences (bound minus free) of G_{LA} and G_{HA} (horizontal axes). The total free energy difference between any two states is independent of the connecting path, so $G_{LA}+G_1=G_0+G_{HA}$. Defining ΔG_{B1} as the net binding free energy arising from the affinity change for an agonist ($=G_{HA}-G_{LA}$), $G_1=G_0+\Delta G_{B1}$. For a receptor with 2 active agonist sites, $G_1=G_0+(\Delta G_{B1}+\Delta G_{B2})$.

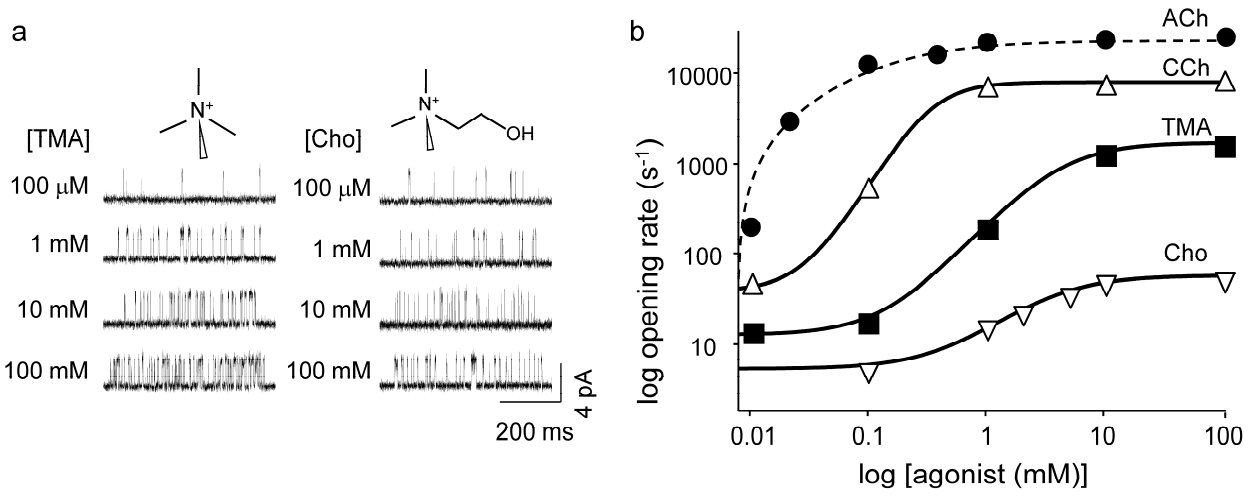

Fig. S2. ($\Delta G_{B1}+\Delta G_{B2}$) for AChRs with 2 WT agonist sites. a. Representative AChR currents at different concentrations of tetramethylammonium (TMA) and choline (Cho), showing clusters of shut-open gating activity. b. Effective opening rate (s^{-1}) vs [agonist], showing the progressive agonist-occupancy of the agonist binding sites. In all cases this rate reaches an asymptote between 1-10 mM, indicating full-occupancy. The solid lines are the fit to the data by Hill equation (n_H^{CCh}=2.1).

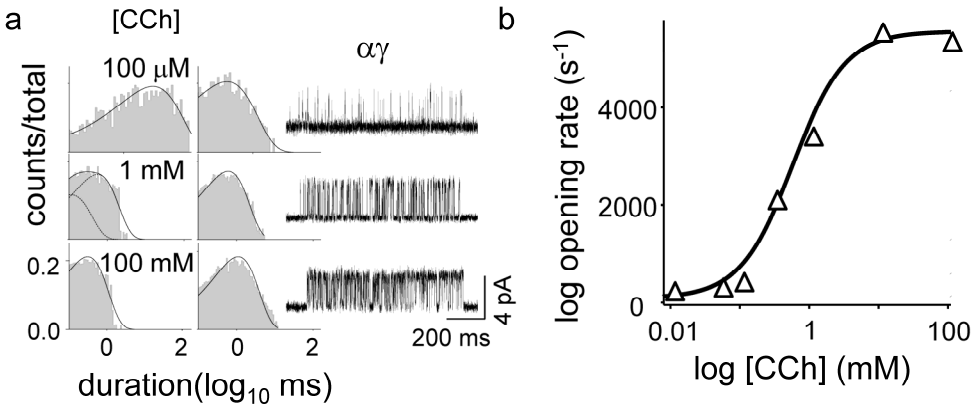

Fig. S3. ΔG_{B1} for AChRs with 1 functional agonist site. a. Interval duration histograms and example currents at different concentrations of CCh in an AChR having only a functional αγ site. (background mutations, βL262S+δP123R; V_m=+70 mV). The solid lines in the interval durations histograms are fits across concentrations by exponential functions. The forward and backward gating rate constants (f_1 and b_1) were determined at 100 mM [agonist] and were used to estimate E_1, G_1 and ΔG_{B1}, as described in the SI methods (Fig. S1). b. Effective opening rate (s^{-1}) vs. the [agonist], showing progressive occupancy of the αγ site by CCh. The solid lines are the fit by the Hill equation (n_H^{CCh}=1.1), which indicates only a single site was functional. For the measured ΔG_{B1} and background G_0 values, see Tables S2 and S9.

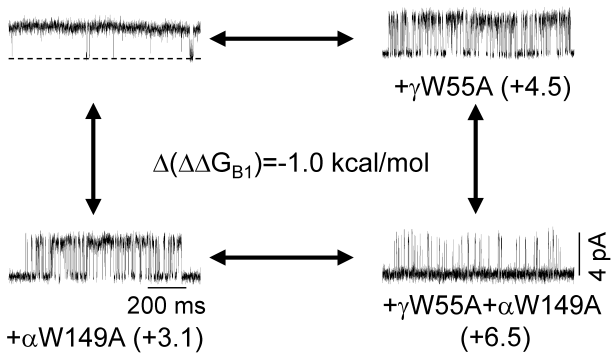

Fig. S4. Coupling free energies between aromatic residues of the binding pocket. Representative current clusters showing the effects of single point mutations at γW55A, αW149A and the double mutation γW55A+αW149A (only αγ site functional). In all cases, the background was βL262S+δL265S+δP123R, [ACh]=100 mM, V_m=+70 mV. The values in parentheses underneath the clusters are $\Delta\Delta G_{B1}$ values (kcal/mol) relative to γW55 (top left). Coupling energy $\Delta(\Delta\Delta G_{B1})$ is defined as the $\Delta\Delta G_{B1}^{double}$- ($\Delta\Delta G_{B1}^{\alpha W149A}$+$\Delta\Delta G_{B1}^{\gamma W55A}$). For other coupling free energies, see Table S5.

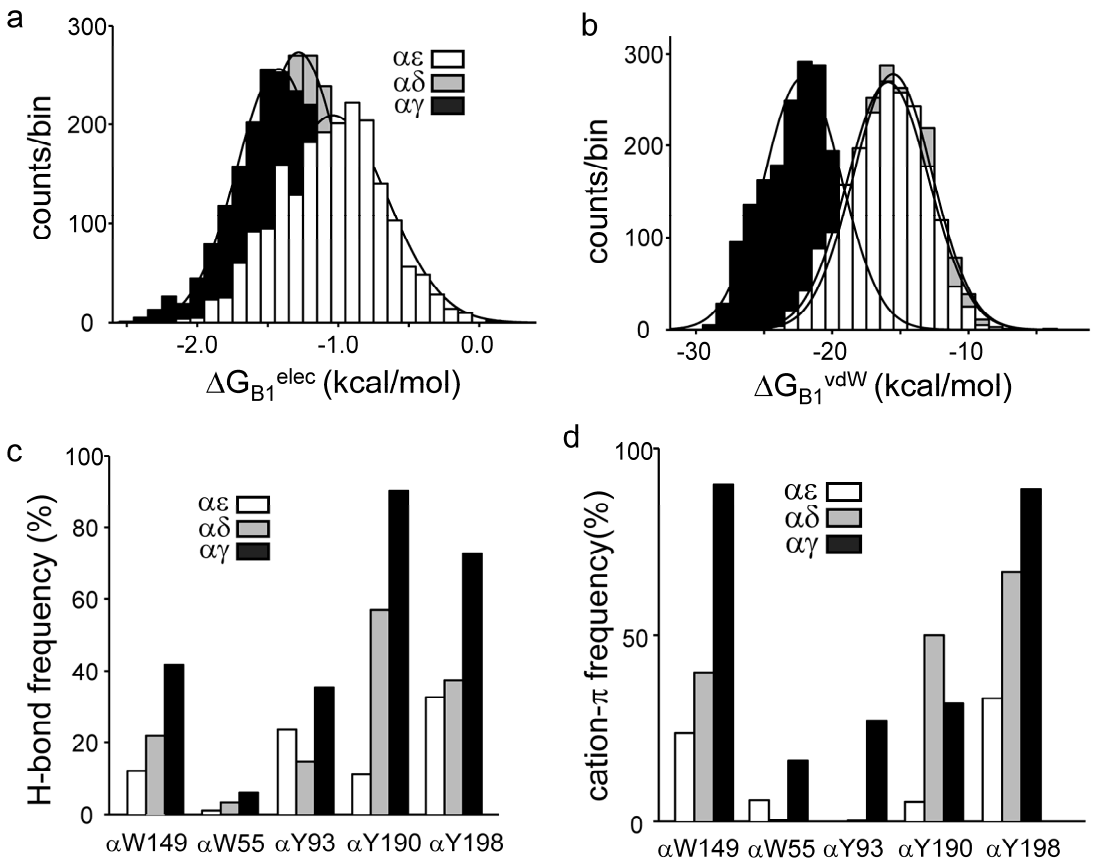

Fig. S5. Energy parameters from MD simulations. a. Distribution of the electrostatic component ΔG_{elec} (kcal/mol) of the ACh-protein binding energy, obtained from the last 10 ns of MD simulations for αε, αδ, and αγ dimers. The distributions were fitted to Gaussian functions. ΔG_{elec} are comparable for all of the binding sites. b. Distribution of van der Waals energy contribution, E_{vdW} at each site. ΔG_{B1}^{vdW} is significantly different at αγ vs αε/αδ. c. Percentage occurrence of hydrogen bond interactions (SI methods) between ACh and the aromatic side chains in the binding pocket. At αγ, side chains have higher probability to form H-bonds with ACh. d. Percentage occurrence of cation-π interactions between the QA and the aromatic residues. αW149 and αY198 maximally participate in cation-π at all the sites, but αY93 and γW55 only do so at αγ.

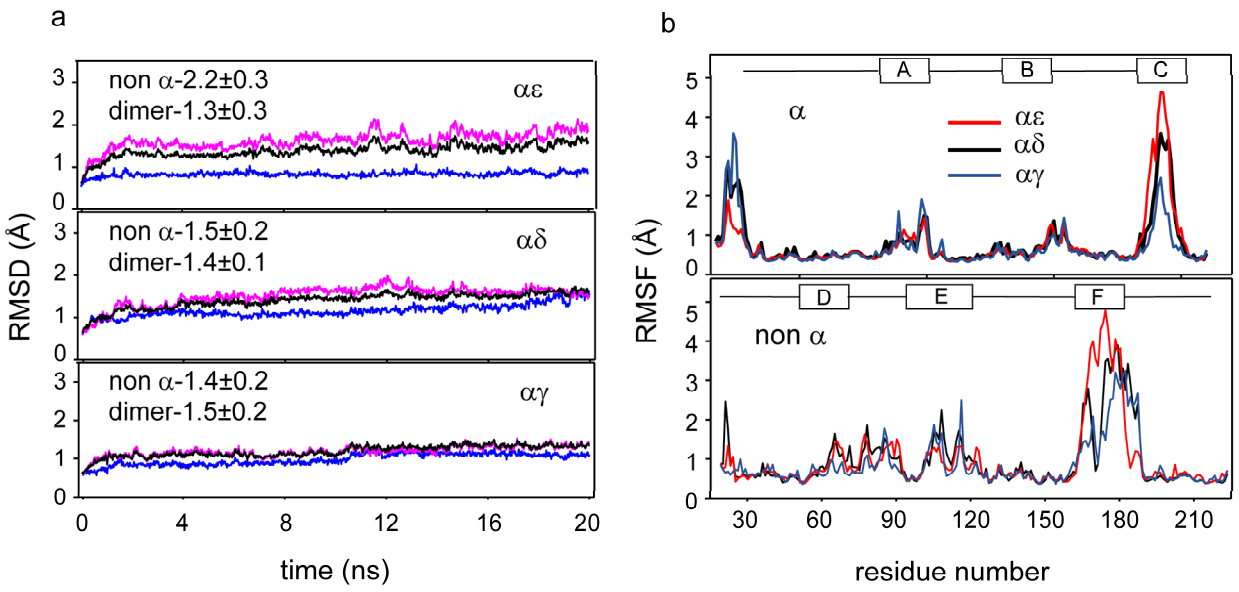

Fig. S6. Comparison of global, simulated structures of each binding sites. a. Representative MD simulation trajectories showing the time evolution of the root-mean-square deviation (RMSD) of the protein backbone atoms for αε, αδ, and αγ dimers (blue, α subunit; black, dimer; magenta, non-α subunit), which equilibrated after 3 ns. The values given (inset) are the average RMSD (Å) for 4 trajectories (S.D.). The average RMSD for the dimer was intermediate between the α- and the non- α side. b. Comparison of residue-wise, root-mean-square fluctuation (RMSF) values for α (top) and non-α (bottom) subunits. Average RMSF for the non-α residues was greater than the α-side. The approximate positions of loops (A-F) are shown as blocks above the traces. As expected, the RMSF was relatively higher at the loops.

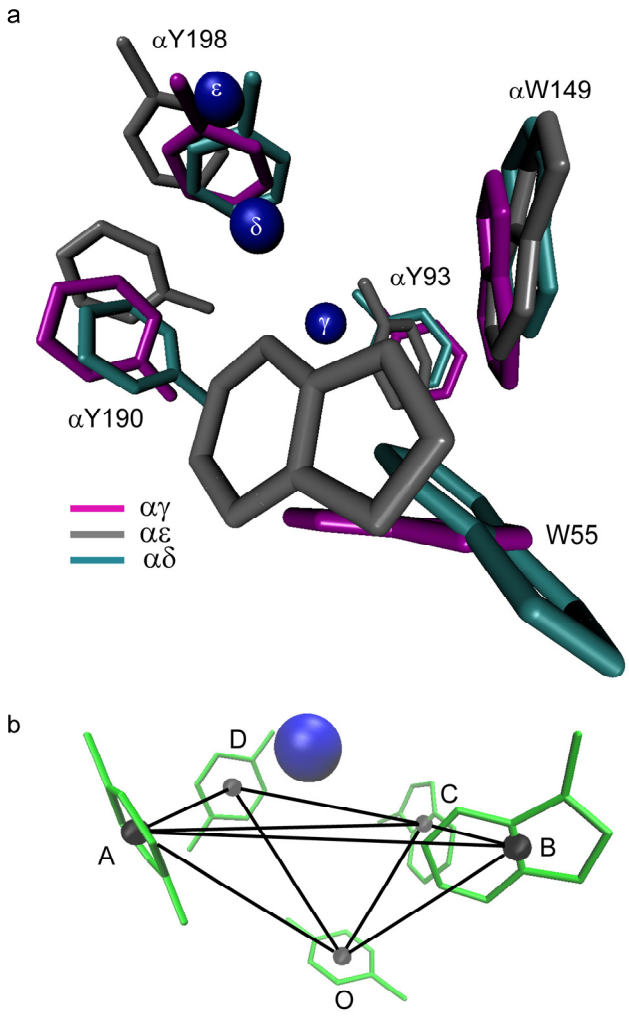

Fig. S7. **Simulated structures of the binding sites**. a. Overlay of the structural models at the αγ (magenta), αδ (cyan) and αε (grey) binding sites, with the Cα carbon atoms of the backbones aligned. The models are snapshots from the last 10 ns of the MD dimer simulations having binding energy and structural parameters comparable to the means of the distributions in Fig. 5 (dimer). Filled blue sphere: N of the QA of ACh. Notice the orthogonal disposition of αW149 and W55 and a more-compact binding pocket at αγ vs αε and αδ, because of the W55 position. b. Model of the αγ site showing 2 virtual tetrahedrons AOCB and ADCO, with O as the common vertex.

REFERENCES

1. Jadey S & Auerbach A (2012) An integrated catch-and-hold mechanism activates nicotinic acetylcholine receptors. *The Journal of general physiology* 140(1):17-28.
2. Purohit P, Bruhova I, Gupta S, & Auerbach A (2014) Catch-and-Hold Activation of Muscle Acetylcholine Receptors Having Transmitter Binding Site Mutations. *Biophysical journal* 107(1):88-99.
3. Sakmann B, Patlak J, & Neher E (1980) Single acetylcholine-activated channels show burst-kinetics in presence of desensitizing concentrations of agonist. *Nature* 286(5768):71-73.
4. Nicolai C & Sachs F (2013) Solving ion channel kinetics with the QuB software. *Biophysical Reviews and Letters* 08(03):1-21.
5. Harris DA, Falls DL, Dill-Devor RM, & Fischbach GD (1988) Acetylcholine receptor-inducing factor from chicken brain increases the level of mRNA encoding the receptor alpha subunit. *Proceedings of the National Academy of Sciences of the United States of America* 85(6):1983-1987.
6. Nayak TK & Auerbach A (2013) Asymmetric transmitter binding sites of fetal muscle acetylcholine receptors shape their synaptic response. *Proceedings of the National Academy of Sciences of the United States of America* 110(33):13654-13659.
7. Jadey SV, Purohit P, Bruhova I, Gregg TM, & Auerbach A (2011) Design and control of acetylcholine receptor conformational change. *Proceedings of the National Academy of Sciences of the United States of America* 108(11):4328-4333.
8. Purohit P, Gupta S, Jadey S, & Auerbach A (2013) Functional anatomy of an allosteric protein. *Nature communications* 4:2984.
9. Gupta S, Purohit P, & Auerbach A (2013) Function of interfacial prolines at the transmitter binding sites of the neuromuscular acetylcholine receptor. *The Journal of biological chemistry*.
10. Hansen SB*, et al.* (2005) Structures of Aplysia AChBP complexes with nicotinic agonists and antagonists reveal distinctive binding interfaces and conformations. *The EMBO journal* 24(20):3635-3646.
11. Li Z & Scheraga HA (1987) Monte Carlo-minimization approach to the multiple-minima problem in protein folding. *Proceedings of the National Academy of Sciences of the United States of America* 84(19):6611-6615.
12. Bruhova I & Zhorov BS (2007) Monte Carlo-energy minimization of correolide in the Kv1.3 channel: possible role of potassium ion in ligand-receptor interactions. *BMC structural biology* 7:5.
13. Tikhonov DB & Zhorov BS (2007) Sodium channels: ionic model of slow inactivation and state-dependent drug binding. *Biophysical journal* 93(5):1557-1570.
14. Bruhova I, Gregg T, & Auerbach A (2013) Energy for wild-type acetylcholine receptor channel gating from different choline derivatives. *Biophysical journal* 104(3):565-574.
15. Foloppe N & Mackerell AD (2000) All-atom empirical force field for nucleic acids: I. Parameter optimization based on small molecule and condensed phase macromolecular target data. *Journal Computational Chemistry* 21:86-104.
16. Phillips JC*, et al.* (2005) Scalable molecular dynamics with NAMD. *Journal of computational chemistry* 26(16):1781-1802.
17. MacKerell AD*, et al.* (1998) All-atom empirical potential for molecular modeling and dynamics studies of proteins. *The journal of physical chemistry. B* 102(18):3586-3616.
18. Martyna GJ, Hughes A, & Tuckerman ME (1999) Molecular dynamics algorithms for path integrals in constant pressure. *Journal of Chemical Physics* 110:3275-3290.
19. Deserno M & Holm C (1998) How to mesh up Ewald sums. I. A theoretical and numerical comparison of various particle mesh routines. *Journal Chemical Physics* 109:7678-7693.

20. Hoover WG (1985) Canonical dynamics: Equilibrium phase-space distributions. *Physical review. A* 31(3):1695-1697.
21. Eriksson MA & Roux B (2002) Modeling the structure of agitoxin in complex with the Shaker K+ channel: a computational approach based on experimental distance restraints extracted from thermodynamic mutant cycles. *Biophysical journal* 83(5):2595-2609.
22. Gilson MK & Honig BH (1988) Energetics of charge-charge interactions in proteins. *Proteins* 3(1):32-52.
23. Im W, Beglov D, & Roux B (1998) Continuum Solvation Model: Computation of electrostatic forces from numerical solutions to the Poisson-Boltzmann equation. *Comput. Phys. Commun.* 111:59-75.
24. Roux B (1997) Influence of the membrane potential on the free energy of an intrinsic protein. *Biophysical journal* 73(6):2980-2989.
25. Brooks BR*, et al.* (2009) CHARMM: the biomolecular simulation program. *Journal of computational chemistry* 30(10):1545-1614.
26. Nina M, Beglov D, & Roux B (1997) Atomic radii for continuum electrostatics calculations based on molecular dynamics free energy simulations. *J. Phys. Chem. B* 101:5239-5248.
27. Morris GM*, et al.* (2009) Autodock4 and AutoDockTools4: automated docking with selective receptor flexiblity. *J. Computational Chemistry* 16:2785-2791.
28. Kuhn B & Kollman PA (2000) Binding of a diverse set of ligands to avidin and streptavidin: an accurate quantitative prediction of their relative affinities by a combination of molecular mechanics and continuum solvent models. *Journal of medicinal chemistry* 43(20):3786-3791.
29. Grazioso G, Cavalli A, De Amici M, Recanatini M, & De Micheli C (2008) Alpha7 nicotinic acetylcholine receptor agonists: prediction of their binding affinity through a molecular mechanics Poisson-Boltzmann surface area approach. *Journal of computational chemistry* 29(15):2593-2602.
30. Ashby JA*, et al.* (2012) GABA binding to an insect GABA receptor: a molecular dynamics and mutagenesis study. *Biophysical journal* 103(10):2071-2081.
31. Humphrey W, Dalke A, & Schulten K (1996) VMD: visual molecular dynamics. *Journal of molecular graphics* 14(1):33-38, 27-38.
32. Bafna PA, Jha A, & Auerbach A (2009) Aromatic Residues {epsilon}Trp-55 and {delta}Trp-57 and the Activation of Acetylcholine Receptor Channels. *The Journal of biological chemistry* 284(13):8582-8588.
33. Purohit P, Bruhova I, & Auerbach A (2012) Sources of energy for gating by neurotransmitters in acetylcholine receptor channels. *Proceedings of the National Academy of Sciences of the United States of America* 109(24):9384-9389.
34. Mitra A, Bailey TD, & Auerbach AL (2004) Structural dynamics of the M4 transmembrane segment during acetylcholine receptor gating. *Structure* 12(10):1909-1918.
35. Mitra A, Cymes GD, & Auerbach A (2005) Dynamics of the acetylcholine receptor pore at the gating transition state. *Proceedings of the National Academy of Sciences of the United States of America* 102(42):15069-15074.
36. Cadugan DJ & Auerbach A (2010) Linking the acetylcholine receptor-channel agonist-binding sites with the gate. *Biophysical journal* 99(3):798-807.
37. Nayak TK, Purohit PG, & Auerbach A (2012) The intrinsic energy of the gating isomerization of a neuromuscular acetylcholine receptor channel. *The Journal of general physiology* 139(5):349-358.